

Collective Modes in Strongly Coupled Binary Liquids

G. J. Kalman^{1*}, Z. Donkó^{1,2}, P. Hartmann^{1,2}, K. I. Golden³, and S. Kyrkos⁴

¹ Department of Physics, Boston College, Chestnut Hill, MA 02467, USA

² Research Institute for Solid State Physics and Optics, Hungarian Academy of Sciences, P. O. Box 49, H-1525 Budapest, Hungary

³ Department of Mathematics and Statistics and Department of Physics, University of Vermont, Burlington, VT 05405, USA

⁴ Department of Chemistry & Physics, Le Moyne College, 1419 Salt Springs Road, Syracuse, NY 13214, USA

Received 17 October 2011, revised 21 March 2012, accepted 21 March 2012

Published online 11 April 2012

Key words Binary Yukawa liquids, wave dispersion, molecular dynamics, QLCA.

We analyze the collective excitations in two- and three-dimensional binary Yukawa systems, consisting of two components with different masses. Theoretical analysis reveals a profound difference between the weakly and strongly correlated limits: at weak coupling the two components interact via the mean field only and the oscillation frequency is governed by the light component. In the strongly correlated limit the mode frequency is governed by the combined mass, where the heavy component dominates. Computer simulations in the full coupling range extend and confirm the theoretical results.

© 2012 WILEY-VCH Verlag GmbH & Co. KGaA, Weinheim

Recently there has been a great interest in the structural properties of binary and multi component Yukawa systems, created by the emergence of the new directions in complex (dusty) plasma [1] and charged colloidal suspension [2] research. Complex plasmas consist of highly charged mesoscopic grains immersed in the background of electrons and ions. It is the presence of the latter that, by screening the bare Coulomb interaction between the grains, generates an effective interaction that in a good approximation can be represented by the Debye-Hückel, or Yukawa potential $\phi(r) = Ze \exp(-\kappa r/a)/r$, where $\kappa = a/\lambda_D$ is the screening parameter, Z is the electric charge, and λ_D is the Debye screening length. The strength of the coupling governing the behavior of the one component Yukawa systems (OCYS) is conventionally characterized by the nominal coupling constant $\Gamma = Z^2 e^2 / akT$ (a is the Wigner-Seitz radius and T is the temperature). Due to the screening ($\kappa > 0$) the effective coupling constant Γ^* (defined in [3–5]) may be substantially smaller. The high value of the grain charge ($Z \gg 1$) ensures that the system is in the strong coupling ($\Gamma^* \gg 1$) regime and consequently in the liquid or solid phase. Both two-dimensional (2D) and three dimensional (3D) Yukawa systems are of interest, although most of the experimental work has focused so far on 2D systems.

The asymmetry between the two components of a *two-component binary Yukawa systems* (BYS) is characterized by three parameters: the mass ratio m_2/m_1 , the charge ratio Z_2/Z_1 , and the density ratio n_2/n_1 . In a complex plasma these parameters are not independent: most importantly, both the m_2/m_1 and the Z_2/Z_1 ratios are determined by the relative grain sizes. Theoretically and in simulation models, of course, these parameters can be separated; indeed they should be so distinguished, in order for one to be able to determine the different physical effects brought about by mass, charge, etc. asymmetries. We have already shown in [6, 7] that for the purpose of calculating the dispersion relation the charge, mass and density ratios can be reduced to two asymmetry parameters $p^2 = (Z_2 n_2)/(Z_1 n_1)$ and $q^2 = (Z_2 m_1)/(Z_1 m_2)$. For the presentation of our results we prefer using dimensionless quantities, which is achieved by introducing the length unit based on the Wigner-Seitz radius as $a = \sqrt{a_1 a_2}$, where $a_A^{2D} = 1/\sqrt{\pi n_A}$ and $a_A^{3D} = \sqrt[3]{3/(4\pi n_A)}$, and the nominal plasma frequency $\omega_1^{3D} = \sqrt{4\pi Z_1^2 e^2 n_1/m_1}$ and $\omega_1^{2D} = \sqrt{2\pi Z_1^2 e^2 n_1/m_1 a}$.

Here we address the issue of the collective spectrum of a BYS, both in 2D and 3D. We find that the spectrum consists of acoustic modes ($\omega \rightarrow 0$ for $k \rightarrow 0$), with coupling dependent “longitudinal” and “transverse” sound velocities $s_{L,T}$ and a number of optic modes (with gap frequencies $\omega_G \neq 0$ for $k \rightarrow 0$). These latter represent

* Corresponding author. E-mail: gabor.kalman@bc.edu, Phone: +1 617 552 3581, Fax: +1 617 552 8478

out-of-phase inter-species oscillations. We study the full excitation mode structure and we investigate how the mass asymmetry, between the two species with $Z_1 = Z_2$ affects the sound speed and the optical mode gap frequencies as the coupling strength Γ is varied from the weak coupling $\Gamma^* \ll 1$ to the strong coupling $\Gamma^* \gg 1$ regime and as the mass ratio m_2/m_1 is varied in a wide range.

Consider now a BYS, with masses and densities m_A and n_A ($A=1,2$), respectively. Each density can be associated with a Wigner-Seitz radius a_A and a nominal coupling constant $\Gamma_A = Z_A^2 e^2 / a_A kT$. In the calculations we parallel the 2D and 3D results.

First we identify the ground state crystal phonon excitation mode structure based on the harmonic lattice approximation. In this calculation a perfect periodic lattice is assumed with N_c particles in the elementary cell. We concentrate on four different systems (see Fig. 1): (a) staggered rectangular (hexagonal) lattice (2D, $\kappa = 1$, $n_2 = n_1$, $m_2 = Mm_1$, $N_c = 2$); (b) honeycomb lattice (2D, $\kappa = 1$, $n_2 = (1/2)n_1$, $m_2 = Mm_1$, $N_c = 3$); (c) BCC lattice (3D, $\kappa = 1$, $n_2 = n_1$, $m_2 = Mm_1$, $N_c = 2$), and (d) FCC lattice (3D, $\kappa = 3$, $n_2 = (1/3)n_1$, $m_2 = Mm_1$, $N_c = 4$). These configurations have been chosen because in the case of Z_1 different from Z_2 at the selected n_2/n_1 ratios they seem to be reasonable candidates for the ground state lattice structure.

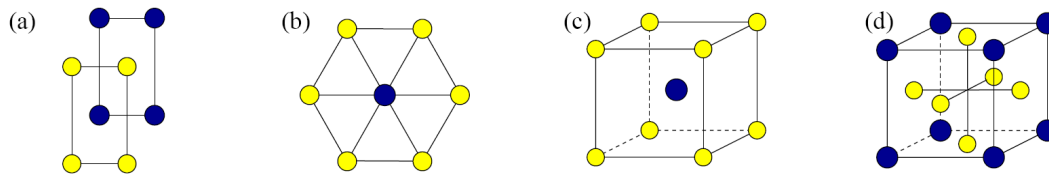


Fig. 1 Schematics of the investigated ground state lattice configurations. For explanation see text.

The lattice dispersion relation is obtained from the dynamical matrix $\mathbf{D}(\mathbf{k})$, which is computed using the standard method (e.g. [8]) of summing contribution from up to 10^6 neighbors:

$$D_{\mu\nu}^{AB}(\mathbf{k}) = \frac{1}{\sqrt{m_A m_B}} \sum_{\mathbf{f}} \Psi_{\mu\nu}^{AB\mathbf{f}} \exp [i\mathbf{k} \cdot (\mathbf{R}_0^{B\mathbf{f}} - \mathbf{R}_0^{A0})], \text{ with } \Psi_{\mu\nu}^{AB\mathbf{f}} = -\frac{\partial^2 \phi^{AB}}{\partial \mu \partial \nu} (\mathbf{R}_0^{B\mathbf{f}} - \mathbf{R}_0^{A0}), \quad (1)$$

where \mathbf{f} runs over unit cells within a large cutoff radius, A and B enumerate the particles within a unit cell, μ and ν are Cartesian coordinates, \mathbf{k} is the wave vector, \mathbf{R}_0 -s are the equilibrium position vectors of the particles.

The maximum number of excitation modes is given simply by the product of the dimensionality number (2 or 3) and N_c . Degeneracy due to structural symmetries can reduce the observed mode number. Illustrative examples for the staggered rectangular and for the honeycomb lattices (Fig. 1a,b) are shown in Fig. 2 for two mass ratios, \mathbf{k} is parallel to the horizontal x -axis as it appears in Fig. 1.

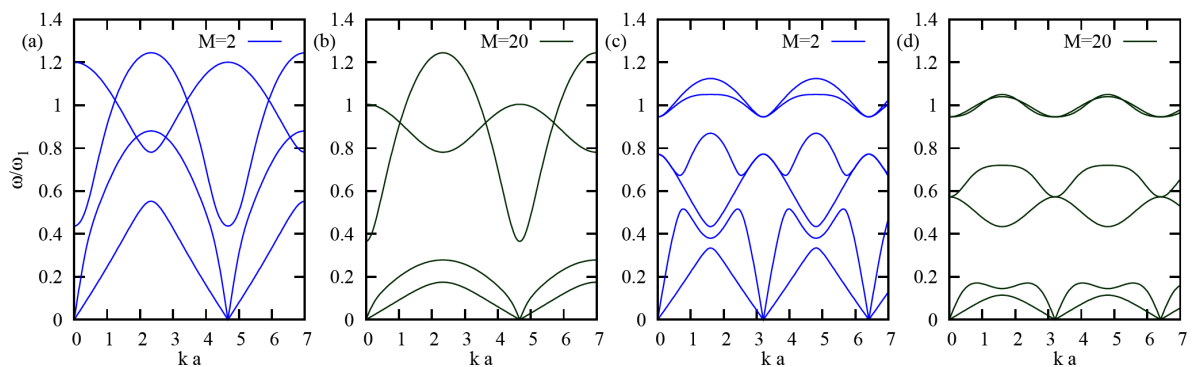


Fig. 2 Dispersion relations for staggered rectangular (a,b) and honeycomb (c,d) lattices at mass ratios $M = 2$ and 20.

For the staggered rectangular lattice there are 2 distinct, “longitudinal” and “transverse”, optic modes (designating these modes thus is justified, in general, in the $k \rightarrow 0$ limit only); for the honeycomb lattice there are 4 optic modes, but the longitudinal and transverse gap frequencies are degenerate, due to the $k \rightarrow 0$ rotational

symmetry of this structure. The honeycomb also illustrates that in the case of $N_c > 2$ a new feature, a mass ratio invariant mode, appears that represents a polarization where the “heavy” particle (m_2) is at rest, and the “light” particles (m_1) move around it. In this case the mass of the heavy species does not come into play, resulting in the observed invariance.

To extend our analysis into the strongly coupled liquid phase we use molecular dynamics (MD) simulations and the quasilocized charge approximation (QLCA) calculations [7,9], matching them with the lattice calculations for $\Gamma \rightarrow \Gamma_m$ the solidification value.

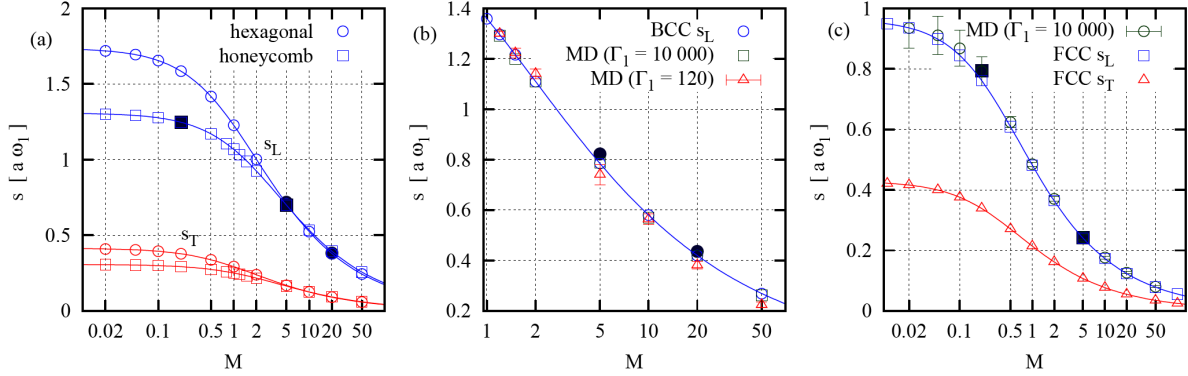


Fig. 3 Longitudinal (s_L) and transverse (s_T) sound speeds vs. mass ratio for: (a) 2D hexagonal (staggered rectangular) and honeycomb lattices, (b) 3D BCC lattice, finite temperature solid (MD at $\Gamma_1 = 10\,000$) and liquid (MD at $\Gamma_1 = 120$), (c) 3D FCC lattice and finite temperature solid. Lines are fitted to lattice values using formula (2). Filled symbols show QLCA results. (taken from [10])

Focusing first on the acoustic modes, in general a good agreement between the different theoretical and numerical approaches is found, as shown in Fig. 3. Sound speeds obtained by lattice summation can be approximated with very high accuracy by the functional form

$$s(M) \propto \frac{s(0)}{\sqrt{1 + \frac{n_2}{n_1} M}}, \quad (2)$$

derived from the QLCA formalism.

We generate 3D and 2D MD simulation data from which we obtain the acoustic speeds, over a wide range of Γ values extending well into the crystalline solid region (see Fig. 4). In the strong coupling limit the QLCA calculations predict that $s_{L,T}$ are governed by the “average atom frequency of the virtual crystal” [11, 12]:

$$s_{L,T}^2 \propto e^2 \frac{\langle Z \rangle^2}{\langle m \rangle} (n_1 + n_2), \quad \text{with} \quad \langle X \rangle = \frac{\sum n_i X_i}{\sum n_i} \quad (3)$$

We can see a rather dramatic decrease of the sound velocity with increasing Γ from the moderately coupled to the strongly coupled regions. For high Γ , near Γ_m the agreement of the MD results with the QLCA predictions is excellent. There is also an almost perfect agreement near Γ_m between these two values pertaining to the liquid and the crystal lattice values. The small discrepancy, visible for the 3D $n_2 = (1/3)n_1$ case can be attributed to the anisotropy of the sound velocity in the FCC lattice: the liquid results correspond to angle-averaged values, while the lattice result is given along the chosen $\{001\}$ direction.

Turning to the optic modes, we observe the general behavior as noted before: gap frequencies $\omega_G = \omega(k \rightarrow 0)$, show pairwise degeneracy for systems with $k \rightarrow 0$ rotational symmetry (honeycomb (see Fig. 2), BCC and FCC). The mass ratio dependence of the gap frequencies is shown in Fig. 5. We also observe the appearance of the invariant frequency for the honeycomb and the FCC.

Our analysis shows that for the system without pairwise degenerate gap (staggered rectangular) the QLCA calculation predicts a single gap with frequency value being the square average of the lattice gaps $\omega_{G,QLCA}^2 = \frac{1}{2}(\omega_{G,1}^2 + \omega_{G,2}^2)$. For the system with one degenerate gap (3D BCC) the QLCA calculation can well reproduce the

lattice value. However, the QLCA approximation in its present form does not reproduce the mass ratio invariant mode, where members of the same species oscillate against each other, at all. Currently, there are no conclusive MD results concerning the behavior of the optic modes in the liquid phase.

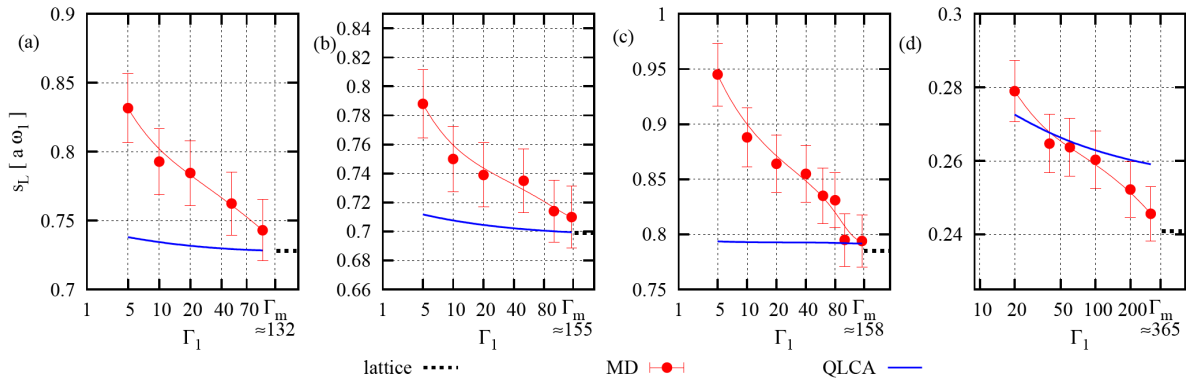


Fig. 4 Longitudinal sound speed vs. Γ_1 in different systems, obtained from MD simulations. 2D: (a) hexagonal (staggered rectangular), (b) honeycomb. 3D: (c) BCC, (d) FCC. $M = m_2/m_1=5$ for all cases. The dotted lines indicate the theoretical high Γ limit; the continuous lines represents the results of the QLCA calculations. (taken from [10])

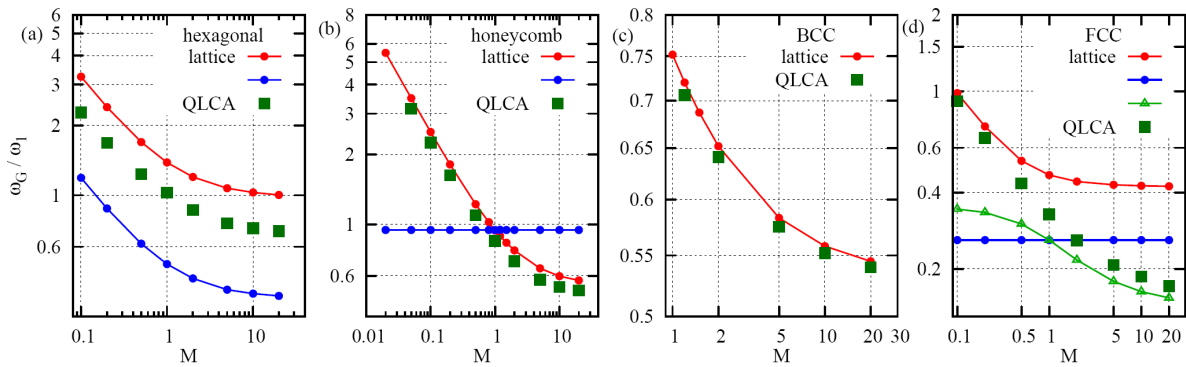


Fig. 5 Gap frequencies vs. mass ratio for all four systems based on lattice and QLCA calculations using pair distribution functions from MD simulations at $\Gamma_1 = 120$.

Acknowledgements This work has been partially supported by NSF Grants PHY-0813153, PHY-0715227, PHY-1105005, PHY-0812956, OTKA Grants K-77653, PD-75113, and HELIOS project (ELI 09-1-2010-0010).

References

- [1] G.E. Morfill and A.V. Ivlev, Rev. Mod. Phys. **81**, 1353 (2009).
- [2] N. Vogel et al., Advanced Functional Materials **21**, 3064 (2011).
- [3] P. Hartmann, G. J. Kalman, Z. Donkó, and K. Kutasi, Phys. Rev. E **72**, 026409 (2005).
- [4] T. Ott, M. Stanley, and M. Bonitz, Phys. Plasmas **18**, 063701 (2011).
- [5] O. Vaulina and S. Khrapak, J. Exp. Theor. Phys. **90**, 287 (2000).
- [6] G. Kalman and K.I. Golden, Phys. Rev. A **41**, 5516 (1990).
- [7] K.I. Golden and G. J. Kalman, Phys. Plasmas **7**, 14 (2000).
- [8] M. T. Dove, Structure and Dynamics – An atomic view of materials (Oxford University Press, 2003).
- [9] Z. Donkó, G. J. Kalman, and P. Hartmann, Journal of Physics: Condensed Matter **20**, 413101 (2008).
- [10] G.J. Kalman, Z. Donkó, P. Hartmann, and K.I. Golden, Phys. Rev. Lett. **107**, 175003 (2011).
- [11] B. Fultz et al., Phys. Rev. B **52**, 3280 (1995).
- [12] H.C. Poon and A. Bienenstock, Phys. Rev. **142**, 466 (1966).